Available online at www.sciencedirect.com
SCIENCE DIRECT®
Journal of Non-Crystalline Solids 351 (2005) 2657–2667
JOURNAL OF NON-CRYSTALLINE SOLIDS
www.elsevier.com/locate/jnoncrysol

Section 3. Dynamics of nano-confined systems

Inelastic neutron scattering for investigating the dynamics of confined glass-forming liquids

B. Frick [a,*], C. Alba-Simionesco [b], G. Dosseh [b], C. Le Quellec [b], A.J. Moreno [c], J. Colmenero [c,d], A. Schönhals [e], R. Zorn [f], K. Chrissopoulou [g], S.H. Anastasiadis [g,h], K. Dalnoki-Veress [i]

[a] *Institut Laue Langevin, 6, rue Jules Horowitz, F-38042 Grenoble, France*
[b] *Laboratoire de Chimie Physique, Université de Paris Sud, Bâtiment 349, F-91405 Orsay, France*
[c] *Donostia International Physics Center, Apartado 1072, 20080 San Sebastiàn, Spain*
[d] *Dpto. Fisica de Materiales UPV/EHU, Apdo. 1072, E-20080 San Sebastiàn, Spain*
[e] *Federal Institute of Materials Research and Testing, Unter den Eichen 87, D-12205 Berlin, Germany*
[f] *Forschungszentrum Jülich, Institute for Solid State Research, D-52425 Jülich, Germany*
[g] *Institute of Electronic Structure and Laser, Foundation for Research and Technology, Hellas, P.O. Box 1527, 711 10 Heraklion Crete, Greece*
[h] *Department of Physics, University of Crete, P.O. Box 2208, 71003 Heraklion, Crete, Greece*
[i] *Department of Physics & Astronomy, The Brockhouse Institute for Materials Research, McMaster University, Hamilton, ON, Canada L8S 4M1*

Available online 2 August 2005

Abstract

Inelastic neutron scattering was employed over recent years to investigate the influence of spatial confinement on the dynamics of glass-forming systems. We review the common phenomena observed by neutron scattering in such different confining hosts like porous glasses, molecular sieves, clays or free standing polymer films, which impose a spatial limitation to the motion of small organic molecules, oligomers or polymers. Near the glass transition temperature the mean squared displacements of the confined molecules show clear deviations from the bulk behavior. The observed increase or decrease of the mean squared displacements confirms the high relevance of the interface interaction near walls of confining media without excluding additional real confinement effects. We show a new comparison of the mean squared displacement for PDMS and PMPS in bulk and in different type of restricting geometries, which evidence a weak influence of the restricting geometry on the local methyl group motion, but a strong influence on the glass transition dynamics, if wall interactions are taken into account. Strong wall interaction is also supported by the intermediate scattering function, measured either by combining neutron backscattering and time-of-flight experiments to cover 3 decades in time from ns to ps or by neutron spin echo, which reveal above T_g an increasing elastic fraction with decreasing pore size and a slowing down of the dynamics. Furthermore we show that a reduction of modes below the Boson peak frequency is a more general feature of confined glass-forming systems.

PACS: 64.70.Pf; 29.30.Hs; 61.25.Hq

1. Motivation

The influence of spatial confinement on the dynamics of condensed matter is of wide interest for both, applications and fundamental understanding. Concerning the latter and for the purpose of searching for a possible correlation length underlying the physics of glass formation – a possible signature of it could be the Vogel–Fulcher divergence of transport properties with decreasing temperature – it seems attractive to study glass-forming systems in spatial confinement.

* Corresponding author. Tel.: +33 476207322; fax: +33 476207688.
E-mail address: frick@ill.fr (B. Frick).

0022-3093/$ - see front matter © 2005 Elsevier B.V. All rights reserved.
doi:10.1016/j.jnoncrysol.2005.03.061

This has been motivation for many experiments and computer simulations on low molecular and polymeric glass-forming systems in spatial confinement of pores or films over recent years (see, e.g., Refs. [1–3]).

The idea seems simple: if a molecular motion is correlated to the motion of molecules in its environment, reaching out to a certain distance, then hypothetically cutting out a smaller range around this molecule should remove some constraints to motion. Spatial limitations in pores or films could have such an effect. In the case that the described constraints would lead to a slowing down of the motion, one would expect the dynamics of the molecules to be accelerated in a spatially limited environment. If a growing correlation length with decreasing temperature would be at the origin of glass formation [4–7], then a spatial limitation should decrease the glass transition temperature T_g, because the molecules would stay mobile down to lower temperature. In fact the glass transition might become suppressed completely below a certain confining spatial length scale.

Of course the described isolated ideal system does not exist and there will always be an interaction of the molecules with the wall. If the effect of this wall would be to block the molecules at the surface of our previously isolated idealized system, then this could counteract the described acceleration of dynamics or if the wall would be highly mobile one could expect an additional acceleration. In the course of years it became more and more evident from experimental investigations and computer simulations that wall interactions are of utmost importance and that T_g can move up or down due to such effects [8]. Just to cite a few examples: adsorption layers are formed and measured in pores, which leads to a slowing down of dynamics; a 'lubrication' of the pores, e.g., by silanization, avoids or diminishes the slowing down. For free-standing polystyrene films the glass transition can shift downwards as much as 70 K from the corresponding bulk value [9,10]. For low molecular weight substances obtaining free-standing films is unrealistic, but recently microemulsion of the PG/AOT/decalin type were proposed to possess nearly 'free' surface conditions [11]. In fact in such a soft confinement the dynamics is accelerated. Finally we also should mention that for nanoporous confinement the pore geometry or the wall roughness can have an important influence on the dynamics (e.g., [12]). Furthermore we should mention in passing that the density within the pore may change, an observation which was recently made by small angle neutron scattering [13,14].

We describe in this paper some aspects where neutron scattering can contribute to understand the influence of confinement. We will shortly introduce the experimental method of inelastic neutron scattering, its information content and how the above-mentioned confinement effects would show up in general. Finally we compile recent experiments on organic liquids and polymers in different confining environments and compare them.

2. Inelastic neutron scattering

Neutron spectroscopy can give a detailed picture of how atoms or molecules move on a microscopic scale. The space and time information comes from the energy and momentum exchanged during a scattering experiment between the neutrons and the sample. The space sensitivity distinguishes neutron spectroscopy from some other spectroscopic methods, like dielectric spectroscopy. Until recently neutron and dielectric spectroscopy were complementary in time range, neutrons probing dynamics on a very short time scale of pico- to nanoseconds and dielectric spectroscopy at seconds to μs times. In recent years both techniques have improved, reaching about 0.1 μs with neutron spin echo spectroscopy and extending the dielectric spectroscopy up to ps. Whereas the space sensitivity remains an advantage of neutron scattering, the dynamic range covered with one dielectric spectrometer is by far wider. This is also why both techniques are often combined, especially in the field of research of the glass transition, because relaxation processes are spread over an extremely large time scale, and dielectric data, mainly spectral shape parameters and relaxation maps, are often used as input or for comparison to inelastic neutron scattering.

The double differential cross section, measured in a neutron scattering experiment, can be written as

$$\mathrm{d}^2\sigma/\mathrm{d}\Omega\mathrm{d}\omega = 1/4\pi \cdot \boldsymbol{k}_\mathrm{f}/\boldsymbol{k}_\mathrm{i}(\sigma_\mathrm{coh}S_\mathrm{coh}(\mathbf{Q},\omega) + \sigma_\mathrm{inc}S_\mathrm{inc}(\mathbf{Q},\omega)), \tag{1}$$

$\boldsymbol{k}_\mathrm{i}$ and $\boldsymbol{k}_\mathrm{f}$ are the incident and final wave vectors of the neutron beam, $\mathbf{Q}$ is the momentum transfer vector, ω the angular frequency to energy transfer $\frac{E}{\hbar}$, Ω the space angle of detection, $S(\mathbf{Q},\omega)$ the so-called scattering functions and σ the scattering cross-sections for coherent and incoherent scattering, respectively.

The scattering law can then be expressed in terms of correlation functions. $S(\mathbf{Q},\omega)$ is related by Fourier transformation (FT) to the intermediate scattering function $S(\mathbf{Q},t)$:

$$S(\mathbf{Q},\omega) = 1/2\pi \int_{-\infty}^{\infty} S(\mathbf{Q},t)\mathrm{e}^{-\mathrm{i}\omega t}\,\mathrm{d}t. \tag{2}$$

Here again one has to distinguish a *coherent* variant of the intermediate scattering function $S_\mathrm{coh}(\mathbf{Q},t)$ referring to the *two-particle* correlations

$$S_\mathrm{coh}(\mathbf{Q},t) = 1/N \sum_{i=1}^{N}\sum_{j=1}^{N} \left\langle \mathrm{e}^{\mathrm{i}\mathbf{Q}\cdot\mathbf{r}_i(0)}\mathrm{e}^{-\mathrm{i}\mathbf{Q}\cdot\mathbf{r}_j(t)}\right\rangle \tag{3a}$$

($\langle\,\rangle$ denotes the thermal averages) and the *self* or *incoherent* variant $S_{\rm inc}(Q,t)$, respectively:

$$S_{\rm inc}(\mathbf{Q},t) = 1/N \sum_{i=1}^{N} \left\langle e^{i\mathbf{Q}\cdot\mathbf{r}_i(0)} e^{-i\mathbf{Q}\cdot\mathbf{r}_i(t)} \right\rangle. \tag{3b}$$

$S(\mathbf{Q},t)$ is related by inverse FT to the van Hove pair-correlation function

$$\begin{aligned} G(\mathbf{r},t) &= \frac{1}{(2\pi)^3} \int_{-\infty}^{\infty} e^{-i(\mathbf{Q}\cdot\mathbf{r}-\omega t)} S_{\rm coh}(\mathbf{Q},t)\, d^3Q\, d\omega \\ &= \frac{1}{N} \sum_{i,j=1}^{N} \delta(\mathbf{r}-\mathbf{r}_i(0))\delta(\mathbf{r}-\mathbf{r}_j(t)) \\ &= \langle \rho(0,0)\rho(\mathbf{r},t)\rangle \end{aligned} \tag{4a}$$

and the self correlation function:

$$\begin{aligned} G_S(\mathbf{r},t) &= \frac{1}{(2\pi)^3} \int_{-\infty}^{\infty} e^{-i(\mathbf{Q}\cdot\mathbf{r}-\omega t)} S_{\rm inc}(\mathbf{Q},t)\, d^3Q\, d\omega \\ &= \frac{1}{N} \sum_{i=1}^{N} \delta(\mathbf{r}-\mathbf{r}_i(0))\delta(\mathbf{r}-\mathbf{r}_i(t)), \end{aligned} \tag{4b}$$

where in Eq. (4a) ρ is the particle density operator (for more details see, e.g., Ref. [15]).

The coherent and incoherent scattering cross sections vary strongly with the kind of atom and can be as high as $\sigma_{\rm inc}(\mathrm{H}) = 80.27$ b for hydrogen, compared to the usually much smaller cross section for other atoms: $\sigma_{\rm coh}(\mathrm{H}) = 1.76$ b, $\sigma_{\rm inc}(\mathrm{D}) = 2.05$ b, $\sigma_{\rm coh}(\mathrm{D}) = 5.59$ b, $\sigma_{\rm inc}(\mathrm{C}) = 0.0$ b, $\sigma_{\rm coh}(\mathrm{C}) = 5.56$ b, $\sigma_{\rm inc}(\mathrm{O}) = 0.0$ b, $\sigma_{\rm coh}(\mathrm{O}) = 4.23$ b, $\sigma_{\rm inc}(\mathrm{Si}) = 0.0$ b and $\sigma_{\rm coh}(\mathrm{Si}) = 2.16$ b [16], just to name a few elements studied in this work ($1\ \mathrm{b} = 10^{-24}\ \mathrm{cm}^{-2}$). In most neutron scattering experiments on organic liquids and polymers the incoherent scattering dominates largely due to the high hydrogen content and therefore the self-correlation function is measured in good approximation. For accessing the pair correlation function one can use completely deuterated molecules or one can use H–D exchange to enhance the contrast for certain molecular motions.

Most of the experimental results presented here were taken on neutron backscattering (BS) or time-of-flight spectrometers (TOF), which measure $S(\mathbf{Q},\omega)$. We also show an example from neutron spin echo (NSE). NSE measures directly $S(\mathbf{Q},t)/S(\mathbf{Q},t=0)$ [17]. The samples discussed in this work were mostly protonated, thus the incoherent scattering dominates and by the presented TOF- or BS-experiments the self-correlation function is accessed. In one case the methyl groups of toluene was protonated and the phenyl ring deuterated, which amplifies the signal from the methyl group, in another case the opposite deuteration was chosen in order to enhance the center of mass motion of the molecule. One fully deuterated toluene sample was used for NSE were the pair correlation function is measured.

3. Information from neutron backscattering

Neutron backscattering instruments like IN10 or IN16 at ILL, Grenoble, France are crystal analyser spectrometers [18] which achieve very high energy resolution in the range of 1 μeV, corresponding to observation times of the order of $t \sim h/E \sim 4$ ns. These instruments are typically used in two different experimental configurations: first, in the elastic fixed window (EFW) mode, in which only elastic scattering processes ($\Delta E \sim 0$; within the instrumental resolution) are counted and second, in the spectroscopic mode, where a moving monochromator is used to periodically apply a Doppler shift to the incident neutron beam. On IN16 an energy transfer range of ±15 μeV can be accessed (see, e.g., Fig. 1).

We consider in the following only incoherent scattering. Under the assumption that all molecular motions are frozen at cryogenic temperatures (e.g., $T < 2$ K) we measure with neutron BS only elastic scattering intensity I_0. Neglecting zero point motions, the integral over the self correlation function and thus the integral over $S_{\rm inc}(\mathbf{Q},\omega)$ should be unity (see Eq. (4b)). At higher

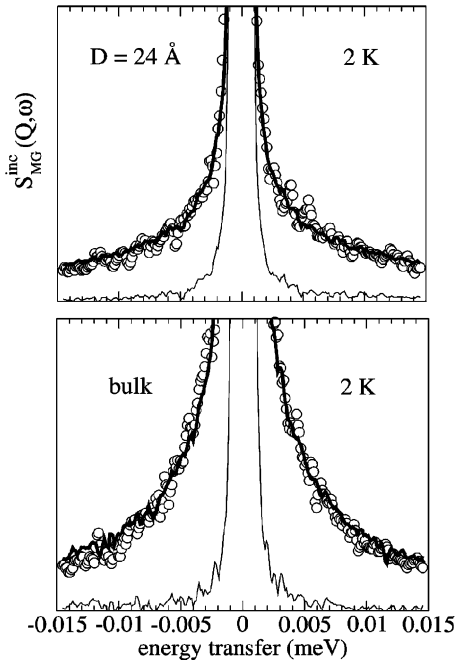

Fig. 1. Confinement effect on the methyl group tunnel splitting of ring deuterated toluene in bulk and confined in MCM-41. The inelastic incoherent scattering function, measured on the backscattering spectrometer IN16, is corrected for the elastic scattering not arising from methyl groups and is plotted on a scale of 3% of the maximum intensity. The thin line is the measured Vanadium resolution function of same geometry. The thick solid line corresponds to a model calculation for the rotational rate distribution [25]. The observed change can be ascribed to a surface layer in confinement which leads to a change in the distribution of local potentials and of the tunnel splitting for methyl groups [28].

temperatures vibrational motions will set on and the incoherent elastic intensity $I = I_0\exp(-\alpha Q^2)$ will drop with temperature like the Debye–Waller factor (DWF), where α is the mean squared displacement (msd), expressed here as $\alpha = 1/3\langle u^2\rangle$ (often $\alpha = 1/6\langle u^2\rangle$ is used). In the EFW mode we measure the elastic scattering as a function of a sample property, e.g., temperature, and extract $\langle u^2\rangle_{\text{eff}}(T)$ (on the ns-time scale) from the Q-dependence of these scans by fitting straight lines to $\ln(I/I_0)$ vs. Q^2. The resulting msd is most sensitive to the low frequency vibrational modes, because in first order and at higher temperatures

$$\langle u^2\rangle_{\text{eff}} \propto k_B T \int_0^{\omega_m} \frac{1}{\omega^2} g(\omega)\,d\omega \propto T \tag{5}$$

holds, where $g(\omega)$ is the density of states [15].

The temperature dependence of the msd should for an harmonic solid at temperatures higher than the Debye temperature approach $\langle u^2\rangle(T) \sim T$. With increasing temperatures other molecular motions set on and linear DWF-fits are no longer strictly valid. The Q-dependence is then modified by the 'elastic incoherent structure factor' (EISF) (see e.g., [19]). The incoherent scattering law for such local motions can be described by

$$S_{\text{inc}}(Q,\omega) = \text{DWF}\left[A(Q)\delta(\omega) + (1 - A(Q))\sum_i L_i(Q,\omega)\right], \tag{6}$$

i.e., by a Q-dependent elastic component (with the EISF $A(Q)$), giving information on the spatial extent of the motion and a term involving one or several spectral functions with a width being proportional to relaxation frequency and a Q-dependence which gives further information on the type of motion [19]. Even in such case the above-mentioned gaussian fits at small Q-values may capture an effective msd, because the initial decay of the EISF is Gaussian-like at small Q. Detailed model fits including a DWF and an additional EISF are of course preferable. At even higher temperatures, where diffusion sets on, the elastic signal disappears and the msd evaluation is only valid after integrating over the diffusional part of the signal. EFW scans or their conversion into an effective msd are very powerful because they give an overview over the onset of different dynamical processes on the ns-time scale. Nevertheless a quantitative analysis is more difficult and the resulting absolute value for the msd has to be taken with some caution, because it presents an average over all sample atoms. In all cases presented here the phonon density of states and the DWF or msd are dominated by the hydrogen atom contributions.

We show in Fig. 2 examples for elastic scans on poly (methyl phenyl siloxane), PMPS ($M_w = 2600$ g mol^{-1}, $M_w/M_n = 1.20$, $T_g = 223$ K), on a silicate matrix and on a nanocomposite containing PMPS. The upper panel for PMPS reveals two steps at the higher Q-values [20]. The first step at low temperatures is due to rotations of the methyl group attached to both polymer chains and which become fast enough for time resolution of the instrument [21,22]. The second step at higher temperatures arises from fast and diffusional motions becoming unfrozen near T_g [23]. From such scans the temperature dependence of the msd is extracted as described above. Examples for the temperature dependence of the msd are shown for PMPS and poly(dimethyl siloxane), PDMS, in the upper part of Fig. 3. This figure also illustrates the influence of averaging on the msd. A first evaluation of the msd near the first step from methyl-group relaxation results in a much lower value of the msd for methyl group protons in bulk PMPS (crosses) compared to bulk PDMS (solid line). This is only because the average includes for PMPS the phenyl ring protons, which are in this temperature range moving too slowly and contribute to the elastic signal. After multiplication of the $\langle u^2\rangle$ values of PMPS by 8/3, the inverse ratio of methyl group protons to the total number of protons in PMPS, we get a good agreement for the methyl group msd of PDMS and PMPS below T_g (compare, for example, the bulk curves; solid line and crosses in the lower part of Fig. 3).

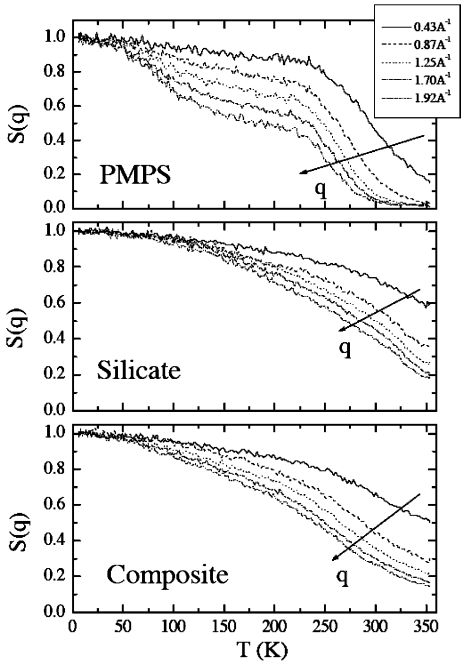

Fig. 2. Elastic temperature scans on bulk PMPS ($M_w = 2600$ g mol^{-1}, $T_g = 223$ K), the silicate matrix (which contains a surfactant) and the intercalated nanocomposite (25% PMPS), measured on IN16 [20]. All data are normalized to the lowest temperature at each Q-value. Bulk PMPS shows a two step relaxation, at low temperature due to methyl group rotation and at high temperature due to the onset of dynamics near T_g. The observed decay for the silicate arises mainly from the surfactant. For the nanocomposite a weak methyl group relaxation step can be recognized as well as the decay near the glass transition.

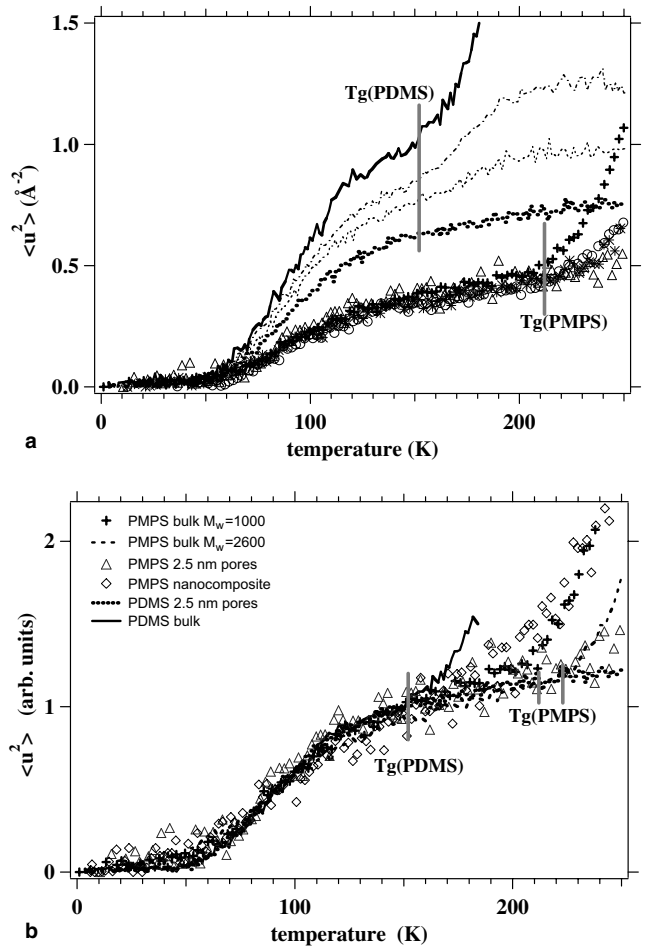

Fig. 3. (a) Pore size dependence of the mean squared displacement for PDMS, $M_w = 1000$ g mol^{-1} (lines in upper group; up to down: bulk, 7.5, 5.0, 2.5 nm), and for PMPS (symbols in lower group: bulk (+), 7.5 nm (○), 5.0 nm (∗) and 2.5 nm (△)). Vertical lines indicate T_g. The divergence of the msd above T_g arises from the onset of fast relaxation and diffusive processes. (b) Rescaled msd as described in the text, showing a similar behaviour for the relaxation of methyl groups in the temperature range up to about 150 K. Minor differences in the width of the step may indicate different potential distributions for methyl group rotation. Above T_g the msd for PDMS (dotted line) and PMPS (△) confined into pores of 2.5 nm is reduced compared to bulk, indicating a slowing down of dynamics. For intercalated PMPS a shift of the msd divergence towards lower temperatures (acceleration) is observed compared to the same bulk PMPS with $M_w = 2600$ g mol^{-1} (dashed line), indicating a speeding up of the dynamics. The divergence in this case is also clearly broadened above T_g.

From BS we obtain more precise spectral information by fitting either the dynamical scattering law S(Q,ω) convoluted with the measured resolution function in frequency space (e.g., Fig. 1) or by Fourier Transformation (FT) of the spectra and fitting the intermediate scattering function $S(\mathbf{Q},t)$ (an example will be given in Fig. 6). As we will see below the BS spectra are often combined with TOF data in order to see a large part of the decay of $S(\mathbf{Q},t)$, because for glasses the spectral function is non-exponential or 'stretched'.

4. Information from neutron time-of-flight spectrometers

TOF spectrometers offer a wide dynamic range (easily several ten meV), but a more coarse energy resolution (50–200 μeV) than BS. The above-mentioned scattering laws are of course valid for TOF spectrometers too and the complementarities of resolution and dynamic range to BS can be used to combine the FT of $S(\mathbf{Q},\omega)$-spectra, i.e. $S(\mathbf{Q},t)$ from TOF and BS which range then over about 4 decades in time. An example will be given in Fig. 6. We also want to add that due to the large dynamic range and due to a large coverage of Q-range one can on a TOF spectrometer measure the phonon density of states g(ω). In incoherent approximation the one phonon scattering law is given by

$$S(\mathbf{Q},\omega) = \langle\sigma_{\mathrm{inc}}\rangle \frac{\hbar^2 Q^2}{2\langle M\rangle} \mathrm{DWF} \frac{g(\omega)}{\omega}(n(\omega)+1), \qquad (7)$$

where the incoherent scattering cross section σ_{inc}, the atomic masses M and the Debye–Waller factor are averaged over all scattering atoms and $n(\omega) = \left[\exp(\frac{\hbar\omega}{kT}) - 1\right]^{-1}$ is the Bose occupation factor. For hydrogenated materials the incoherent H-contribution is by far the dominant term. Examples for the density of states, presented as $g(\omega)/\omega^2$ in order to stress deviations from a Debye behaviour ($g(\omega) \sim \omega^2$) will be given in Fig. 8.

5. Information from spin echo

Neutron spin echo, in contrast to BS and TOF, NSE measures $S(\mathbf{Q},t)/S(\mathbf{Q},0)$. Both, coherent and incoherent scattering can be explored in principle, as long as one component is dominating [18]. Here we show only an example for coherent scattering, thus giving information on the pair correlation function (see Fig. 7). With NSE the intermediate scattering function can be investigated over 2–3 decades in time without combining it with other instruments or setups.

6. Methyl groups as a local probe of confinement effects

Methyl groups can locally reorient around the 3-fold axis of the C–CH_3 bond. At high temperatures, if the thermal energy is sufficiently high to overcome the potential barriers, e.g., $V(\phi) = V_0(1 - \cos(3\phi))/2$, classical hopping over the barriers takes place and gives raise to a quasielastic line in neutron scattering. At very low temperatures, in the quantum regime, there is a tunnel probability to find the MG protons in either of the potential minima and the torsional ground state is split. This tunnel splitting, which follows approximately an exponential dependence on the height of the barrier to

rotation, presents an extremely sensitive probe of the local environment at temperatures of ~1 K and it has often the correct energy to be observed by n-BS or TOF. For crystals it leads then to sharp inelastic excitations in $S(\mathbf{Q},\omega)$ [24]. For glasses a wide distribution of tunneling states is expected, and this inelastic scattering appears then as 'quasielastic-like' wings in the spectra [25–27]. Therefore it is interesting to use the tunnel splitting also as a test probe for the local environment of liquids confined into pores.

In fact it was found for toluene-d5 that the distribution of tunnel barriers clearly changes in confinement [28], which can be seen by bare eye from the 'quasielastic' wing (Fig. 1). A quantitative data evaluation indicates an important shift of the energy barriers to lower frequencies, which was interpreted by taking two toluene phases into account: an unmodified bulk fraction and a surface layer fraction of at least 7 Å thickness [28]. Thus in this analysis there was no need to consider an intrinsic spatial confinement effect on the local methyl group tunneling of the frozen bulk fraction, but a surface layer contribution was sufficient to explain the difference between bulk and confined toluene in the quantum regime.

At higher temperatures, in the classical hopping regime, the study of a confinement effect onto the MG dynamics becomes more difficult because of the onset of other molecular motions near the glass transition temperature T_g, especially if T_g is low like for toluene (T_g(bulk) = 117 K). In some cases the methyl group dynamics is separated from the dynamics setting on near T_g. As an example we show in Fig. 2 the elastic scans [20] for PMPS in bulk and confined in a nanocomposite of PMPS intercalated in organically modified silicate [29]. Bulk PMPS ($M_w = 2600$ g mol^{-1}; $T_g = 223$ K) shows a clear decrease of the elastic scattering below T_g, which is due to the fact that the methyl group dynamics becomes faster than the time of ~4ns corresponding to the experimental resolution. The second step can clearly be associated with the dynamics setting on above T_g. The additional scans in Fig. 2 show the temperature and Q-dependence of the elastic intensity for the silicate matrix (the observed decay can be ascribed to the protonated surfactant in the sample) and for the PMPS containing nanocomposite.

Another polymer with a relatively good separation of MG-dynamics and T_g-processes is PDMS [30–36]. In Fig. 3 we compare the effective msd of PDMS and PMPS in the T-range where methyl group rotations pass the time window of IN16. The lines in the upper figure belong to PDMS ($M_w \approx 1000$ g mol^{-1}, $T_g = 212$ K) and summarize again the [33–36] influence from confinement in the low temperature range. PDMS shows in the range below T_g (vertical lines) a much more pronounced confinement effect on the methyl group motions than PMPS, as described in Ref. [33].

In the lower part of Fig. 3 the effective msd values for PMPS are multiplied with 8/3, assuming that only 3/8 of the protons in PMPS participate in the observed relaxation. This allows for a better comparison of PMPS and PDMS. The bulk PDMS (solid line in the lower figure) and bulk PMPS (crosses and dashed line) superimpose below T_g. Regarding the confined polymers, we present in the lower part of Fig. 3 for clarity only the data for the most extreme confinement within the 2.5 nm pores. The confined PMPS data in the upper part of Fig. 3 did already superimpose with the bulk, thus a multiplication with 8/3 is appropriate to superimpose PMPS in 2.5 nm pores (Δ) with the other curves below T_g. As expected from the upper panel in Fig. 3, the data for PDMS in 2.5 nm pores (dotted line) will not fall on the same curve. However, we find here that a rescaling with a factor 1.5 will superimpose them again with the bulk PDMS curve (solid line) in the low temperature range. The factor $f = 1.5$ which has to be applied to the data of PDMS in 2.5 nm pores might be rationalized assuming a frozen surface layer. Under this premise we can estimate that $f_s = 1 - 1/f = 1/3$ of the protons are frozen, whereas $f_R = 2/3$ are contributing to the relaxation. For cylindrical pores with diameter 2.5 nm we calculate then a frozen layer thickness of $d_S \sim 0.23$ nm (compared to 0.7 nm deduced for toluene from tunneling).

Along the same line of interpretation we may then conclude that PMPS, in contrast to PDMS, does not form a surface layer in the pores or at least a much thinner one. This would also be consistent with the intermediate scattering function $S(\mathbf{Q},t)$, resulting from a combination of TOF and BS at $T = 120$ K, which shows for PDMS at long times a stronger confinement induced elastic fraction than for PMPS [33]. An adsorption layer would give a constant fraction for $t \to \infty$ in $S(\mathbf{Q},t)$ (see Figs. 8 and 9 in Ref. [33]). An alternative explanation is offered in the paper by Schönhals [33] in terms of a tendency of PDMS to crystallize or to order locally near the pore surfaces. On the other hand dielectric data showed a separate peak for PMPS, which was interpreted as arising from a surface layer and such an additional peak was not found for PDMS. This controversial finding has still to be clarified.

Finally we add to the lower panel of Fig. 3 an extremely confined PMPS ($M_w = 2600$ gmol^{-1}), intercalated within the galleries of a nanocomposite (open diamonds, $\diamond$) and compare it to the same molecular weight bulk PMPS (dashed line). In this case PMPS is enclosed in a 2-dim confinement within a spacing of about only 1 nm. Here the scale factor can not be interpreted quantitatively, because the silicate host contains protonated surfactants, the strong scattering of which was corrected, but not rigorously. It should be noted, however, that the quasielastic spectra of the pure silicate do not show any relaxation process at temperatures around

100 K [20], that is the surfactant molecules do not exhibit any relaxation at these low temperatures as long as there is no polymer present in the galleries. It seems also that the step related to the methyl group rotation could be somewhat broader.

Concluding on the methyl group rotation in the temperature range below about 140 K and below T_g for all polymers, all msd for PDMS and PMPS polymers in bulk and confinement superimpose fairly well. This suggests a similar activation energy for the MG rotation in both polymers. Minor changes in the shape or the width of the step may indicate a difference in distribution of local potentials, which seem to be most pronounced for the nanocomposite. For PDMS confined in 2.5 nm pores a necessary scaling factor is rationalized by assuming an adsorption layer of about 0.8 nm. For intercalated PMPS, due to experimental difficulties, an arbitrary scaling factor was applied. The temperature range above T_g will be discussed below.

7. Glass transition in confinement

Up to here we have used the methyl groups as a probe for confinement. If we want to study the glass transition dynamics itself, the scattering contributions from the methyl group rotation may be disturbing and rather difficult to separate. With neutron scattering we can then use the contrast variation and we can exchange the methyl group hydrogen by deuterium. The contributions to the scattering from the dynamics of the methyl groups can thus practically be avoided.

This possibility was used in the study of the confinement effect of toluene, by using toluene-d3 [37]. Fig. 4 shows an example of the temperature dependence of the mean squared displacement for toluene-d3 in MCM-41 matrices of different pore size. The data were taken at the IN16 backscattering spectrometers at ILL. The first observation is that no influence of the MG-dynamics is seen on the elastic scan data, which possibly should show up as a step in the low temperature range (see above). The second observation is that there is no clear divergence of the msd near the glass transition temperature. A strong divergence of the msd near T_g is a well known feature observed by inelastic neutron scattering on glass-forming systems [23,38] and it is related to the onset of fast ps motions and diffusion processes at higher temperatures. For toluene-d3, where we study mainly the phenyl ring dynamics, we observe a more continuous divergence setting on already below T_g. However, for a decreasing host pore size the divergence of the msd is shifted towards higher temperatures. This behaviour is opposite to what is expected from a true confinement effect onto the glass transition, where an acceleration of the dynamics with respect to bulk and thus a decrease of T_g is expected. The explanation is that

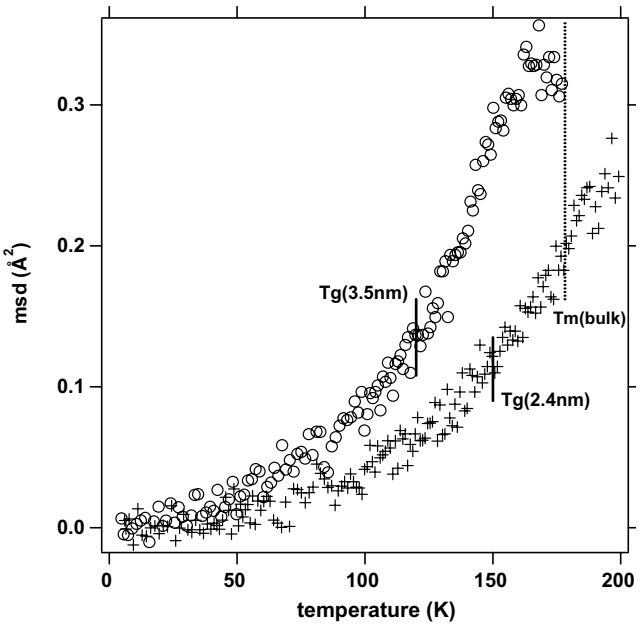

Fig. 4. Pore size dependence of the mean squared displacement of toluene-d3 measured on IN10 in MCM-C16 (3.5 nm pore size) and MCM-C10 (2.4 nm pore size) as a function of temperature. The methyl group is deuterated in order to remove its relaxation contribution. A continuous increase of the msd is observed even below T_g, measured by DSC. The msd decreases with decreasing pore size and T_g shifts to higher temperature [41].

toluene-d3 in these untreated pores interacts with the pore walls and forms a more rigid layer [37]. The surface interaction has the effect to slow down the molecular motions and to transmit this slowing down quite far into the pore volume, a view which is also supported by MD-simulations [37]. For toluene in pores as small as 2.4 nm these surface effects dominate over the finite size effects (see Fig. 1 in [37]).

The importance of surface effects is also known from studies of thin polymer films. A strong decrease of T_g by as much as 70 K is observed for free standing PS films, which do not interact with the surface but with air only (see e.g., [9,10]). A T_g increase has been observed for supported PMMA films on a much more strongly interacting substrate. Here we continue to use the temperature dependence of elastic scans or of the msd as a mean to analyze the relaxation on a ns-time scale. Neutron backscattering experiments on IN16 on a stack of 140 free standing PS films ($M_w = 1{,}250{,}000$ g/mol) of thickness 55 ± 2 nm, compared to a stack of 70 free standing films with 107 ± 2 nm and bulk PS revealed that the msd for the 55 nm films was higher than for the thicker films [39]. Fig. 5 shows a comparison of the temperature dependence for the different films measured. Though this experiment was at the limit of what is feasible for inelastic neutron scattering (total sample thickness of ~7.6 μm), it revealed a clear acceleration effect for the microscopic dynamics in these

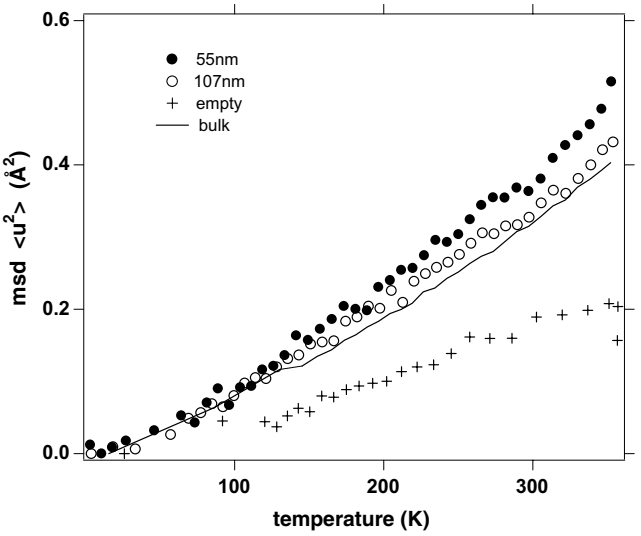

Fig. 5. Mean squared displacement of a stack of free standing polystyrene films ($M_w = 1{,}250{,}000$ g/mol) with 55 nm thickness each(filled circles), 107 nm each (open circles) and bulk (line) deduced without subtraction of background and holder. Crosses show the values deduced from the latter [39].

2-dimensionally confining films, in agreement with T_g measurements [9].

Having seen the importance of surface effects on the relaxations near T_g, we return to the lower part of Fig. 3. The vertical lines indicate the glass transition temperatures of PDMS and PMPS (two T_g values due to different M_w). As can be seen from the figure, the confinement effect on PDMS is to reduce the msd drastically (compare solid and dotted line) [33]. For PMPS in confining pores there is no marked influence at all in the region of methyl group rotations, but a reduction or shift of the msd divergence above T_g towards higher temperatures (crosses and open triangle). In contrast, for intercalated PMPS there is a pronounced acceleration of the dynamics, the divergence of the msd being shifted down in temperature (dashed line and open diamonds). In spite of the uncertainty related to the subtraction of scattering contributions from the surfactant, we can speculate that the intercalated PMPS is in contact with the highly mobile surfactant layer and therefore its dynamics near and above T_g may be accelerated (different subtraction procedures influence the msd mainly above the temperature range shown, but are consistent with an acceleration effect). In contrast, for PDMS an immobile adsorption layer is formed, which slows down the molecular motions. Interface effects thus strongly influence the behavior in confinement and extend relatively far into the confined volume. A closer look on the high temperature data suggests that besides a small acceleration there is an important broadening of the relaxation phenomena in temperature [20].

Spectral information on the intermediate scattering function from 4 decades in time can be obtained by combining BS and TOF experiments. After inverse FT of the dynamic scattering law $S(\mathbf{Q},\omega)$ and after division by the inverse FT of the resolution function $R(\mathbf{Q},t)$, which is usually measured at low temperature on the same sample, one obtains the intermediate scattering function $S(\mathbf{Q},t)$. An example is shown in Fig. 6 where data from IN6 and IN16 are combined to depict the Q-dependence of PMPS confined in 2.5 nm pores at $T = 360$ K, a temperature range where segmental relaxation should be visible. The disentanglement of the different dynamic contributions to $S(\mathbf{Q},t)$, that of the methyl groups (probably very fast and contributing to the initial decay), of the surface layer (which may become sufficiently mobile at these high temperatures to be seen in the present time window) and that of the segmental relaxation (probably main contribution in the presented time window) will be subject of a future publication [40].

Finally we show an example for NSE measurements on deuterated toluene [41]. In this case the intermediate scattering function gives information on the pair correlation function. Fig. 7 compares deuterated toluene for the bulk and for three different pore sizes, 4.7 nm, 3.5 nm and 2.4 nm [41]. The measuring temperature was $T = 180$ K for the bulk and for the different confined samples, but the bulk measurement shown (crosses) were taken on a TOF spectrometer (MIBEMOL at LLB, Saclay, France). Two aspects can be clearly seen: first, at long times the intermediate scattering function reaches a finite value, an indication for the existence of a surface layer, similar to what was shown above for TOF/BS data on PDMS [24], and second, a slowing down of the structural relaxation can be evi-

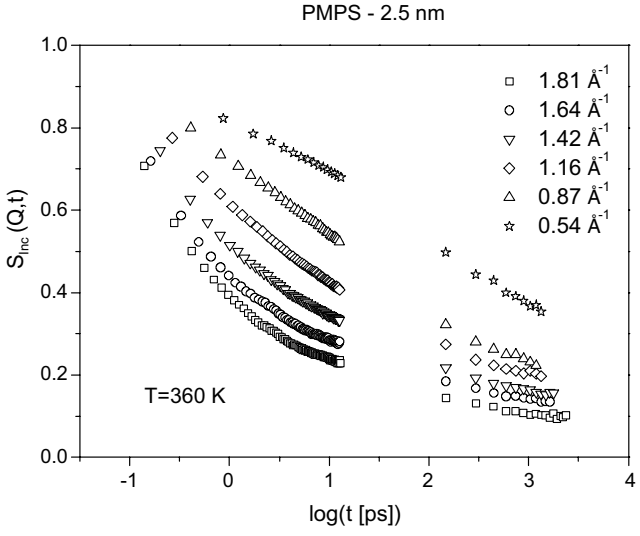

Fig. 6. Intermediate scattering function $S_{inc}(\mathbf{Q},t)$ for PMPS confined to nanopores of 2.5 nm at $T = 360$ K for different scattering vectors: (□) $Q = 1.81$ Å^{-1}, (○) $Q = 1.64$ Å^{-1}, (▽) $Q = 1.42$ Å^{-1}, (◇) $Q = 1.16$ Å^{-1}, (△) $Q = 0.87$ Å^{-1} (☆) 0.54 Å^{-1}. The points between 0.5 ps and 20 ps originate from the Fourier transform of IN6 data; those at $t > 150$ ps from that of IN16.

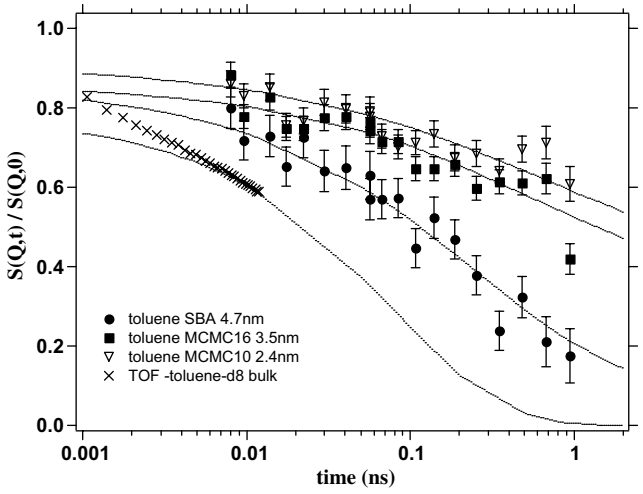

Fig. 7. Pore size dependence of the intermediate scattering function of toluene-d8 measured by NSE on IN11C at $T = 180$ K and $Q = 1.26$ Å^{-1}. Symbols: toluene-d8; Bulk (×), 4.7 nm pores in SBA-15 (filled circles), 3.5 nm pores in MCM-41 (filled squares) and 2.4 nm pores in MCM-41 (triangles). Crosses are TOF data from MIBEMOL. Lines are fits with a stretched exponential function plus an elastic fraction due to interface [41].

denced by fitting the curves (dotted lines) with stretched exponential functions (structural relaxation) including an elastic fraction (adsorbed layer).

As the last topic we want to mention the behavior of the Boson peak (Bp) of confined glass-forming systems. The origin of the Bp and its relevance for the understanding of the glass transition is still debated. Therefore experimental results testing the change of the Bp as a function of parameters like pressure [42–44], molecular weight [45] or spatial confinement [46–48] are needed. The most pronounced influence of spatial confinement

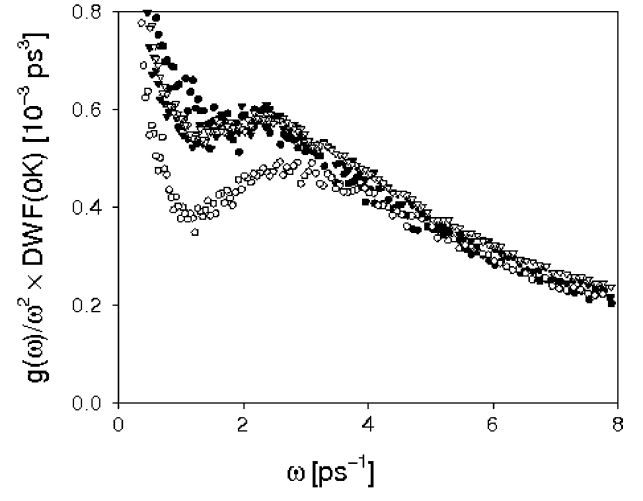

Fig. 8. Density of states $g(\omega)$ divided by ω^2 showing the behaviour of the Boson peak of PDMS at $T = 100$ K in confinement. Compared are bulk (filled circles), PDMS in 7.5 nm pores (open triangles), PDMS in 5 nm pores (filled squares) and PDMS in 2.5 nm pores (open diamonds) (after [48]).

on the Bp is the reduction of low frequency modes below the Bp maximum. A possible origin was discussed in terms of cut-off frequencies for transversal sound velocities in spatial confinement, but gave only qualitative agreement, and a consideration of a surface layer could only explain half of the suppression effect [46]. For PDMS at $T = 100$ K the observed low frequency suppression in confinement was weak for pores of 5.0 nm and 7.5 nm, but very pronounced for pores of 2.5 nm size. Fig. 8 shows the dynamic scattering law for PDMS, where the suppression effect can be seen clearly for the smallest confinement of 2.5 nm. A similar suppression effect is seen for PMPS [49]. Thus an investigation of the Boson peak suggest as well that both contributions, a real confinement effect and an additional surface layer have to be taken into account [48].

8. Discussion

Inelastic neutron scattering data on the low molecular glass former toluene and the oligomers PDMS and PMPS in small confining pores show clearly the existence of a less mobile surface layer. Methyl groups, which can be considered as a local probe, sense the different environments. In the quantum region of methyl group rotational tunneling the inelastic wing of the dynamic scattering law of toluene arises from a distribution of potentials, which can be measured by neutron backscattering and which leads to an unambiguous confinement effect changing the apparent width of the signal. A combined surface layer of at least 7 Å and an unmodified bulk phase describe the data well. In the classical regime, where methyl group rotation leads to a quasielastic signal, elastic scan data for PMPS and PDMS can again be understood assuming the formation of a pore surface layer for PDMS. From the elastic scans a weak influence of the confinement on the methyl group rotations would be expected if the surface layer is taken into account. In fact the intermediate scattering function of PDMS at $T = 120$ K (see Ref. [33]) shows only a weak increase of the relaxation time with increasing confinement.

In contrast for temperatures higher than bulk T_g, there is a clear confinement effect on the effective msd for all polymers, both confined in pores and in nanocomposites. The msd for PDMS and PMPS is reduced with increasing confinement, whereas it seems to be increased for PMPS intercalated in organically modified silicates. The latter should be taken with care, because the protonated surfactant also contributes to the dynamics in the temperature range above 180 K (Fig. 2, middle) [20]. Due to the strong contribution of the surfactant dynamics it was not possible as yet to clearly separate the contribution of PMPS in the measured quasielastic spectra. Moreover, when deuterated

(instead of protonated) surfactants were utilized to organophilize the montmorillonite clays, the PMPS did not intercalate within the silicates. For this we turned to hydrophilic homopolymers (like polyethyleneoxide), which can intercalate in the absence of surfactants; their dynamics under confinement will be reported separately [50]. Yet, PMPS is within the galleries in contact with a highly mobile surfactant layer and therefore the deduced acceleration effect seems plausible and can be compared with the acceleration observed for PG enclosed in microemulsion droplets [11]. An acceleration of the dynamics increase of the msd is also found under free surface conditions for a stack of free standing films of very high molecular weight PS [39], though here the smallest film thickness is about a factor 10 higher and the origin of the observed acceleration may be even more complex (see e.g., [10]). Due to lack of intensity it was not possible to observe the acceleration effect for the free standing PS films directly in the dynamic scattering law $S(\mathbf{Q},\omega)$. From other reasons the situation is similar for the nanocomposites, where the msd seems to be increased.

For the results of glass formers confined in pores the measurement of spectra was in all cases possible and a slowing down of the dynamics above T_g is always observed on the time scale shorter than nanoseconds. This can be deduced from both, the msd and the intermediate scattering function. In the case of the polymers shown here, the contribution of the methyl groups complicates a quantitative data evaluation, but it becomes feasible if the methyl group dynamics is sufficiently well characterized. The most pronounced effect is seen for toluene-d3, were the methyl group is deuterated to enforce the contrast for the center of mass motion of the molecule. From the msd a clear shift towards higher temperatures can be observed, which also corresponds to the observation by DSC. Unfortunately equivalent measurements of the msd for toluene-d3 in bulk do not exist. Such a strong shift is not detected for the msd corresponding to PDMS and PMPS in confinement. The interaction of toluene with the pore walls seems to be stronger than in the case of oligomers. Also the layer thickness seems to be larger for the aromatic molecule, which may indicate a more effective ordering among the different toluene atomic layers leading to an increased coupling of wall effects into the pore. Along the same line the stronger tendency to order for PDMS compared to PMPS [33] may explain the differences seen in both, the msd and the intermediate scattering function for both polymers. For an explanation why inelastic neutron scattering observes a slowing down of the dynamics for the confined oligomers PDMS and PMPS and dielectric relaxation finds an acceleration we refer to Ref. [33]. To resolve this apparent discrepancy a combined analysis of neutron scattering and dielectric data is required which is in progress [40].

9. Conclusion

Inelastic neutron scattering data on toluene, oligomers of PDMS and PMPS confined in pores or layers of nanocomposites and free standing polymer films all show confinement effects on a time scale shorter than nanoseconds. Wall effects are detected by analyzing as a local probe the methyl group dynamics, which is especially sensitive in the quantum regime via the study of the tunnel splitting. Mean squared displacements show in the low temperature range only a weak influence by spatial confinement after correction for a rigid surface layer, consistent with the observation of an elastic fraction in the intermediated scattering function. Above the glass transition temperature, where structural relaxations are expected, the mean squared displacement becomes either reduced or enhanced, depending if the wall properties are more rigid (adsorption) or more dynamic (free surface, mobile interface). For toluene-d3 in untreated pores the decrease of the msd is observed to be particularly strong and for a free standing film and a nanocomposite an increase of the msd is suggested as a function of decreasing spatial dimension of the confinement. The intermediate scattering function for deuterated toluene and for protonated PDMS and PMPS in pores is clearly slowed down due to spatial restrictions, but a more quantitative result still needs a more detailed analysis in order to separate wall effects from intrinsic spatial confinement effects. In some cases the dynamics of protonated methyl groups renders the analysis even more complex.

References

[1] B. Frick, H. Büttner, R. Zorn (Eds.), J. Phys. IV 10 (2000) (EDP Sciences, Les Ulis, France).
[2] B. Frick, M. Koza, R. Zorn (Eds.), Eur. Phys. J. E 12 (2003) 3.
[3] J.T. Fourkas, P. Levitz, M. Urbakh, K.J. Wahl (Eds.), Proceedings of the MRS, vol. 790, MRS, Boston, 2003, p. 336.
[4] G. Adam, J.H. Gibbs, J. Chem. Phys. 43 (1965) 139.
[5] E. Donth, The Glass Transition, Springer, Berlin, 2001.
[6] P. Scheidler, W. Kob, K. Binder, Europhys. Lett. 59 (2002) 701.
[7] P. Scheidler, W. Kob, K. Binder, Eur. Phys. J. E 12 (2003) 5.
[8] G.B. McKenna, J. Phys. IV 10 (2000) 343.
[9] J.A. Forrest, K. Dalnoki-Veress, Adv. Colloid Interface Sci. 94 (2001) 167.
[10] J.A. Forrest, Eur. Phys. J. E 8 (2002) 261.
[11] L.M. Wang, F. He, R. Richert, Phys. Rev. Lett. 92 (2004) 95701.
[12] B. Coasne, R.J.M. Pellenq, J. Chem. Phys. 120 (2004) 2913.
[13] D. Morineau, R. Guegan, Y.D. Xia, C. Alba-Simionesco, J. Chem. Phys. 121 (2004) 1466.
[14] D. Morineau, Y.D. Xia, C. Alba-Simionesco, J. Chem. Phys. 117 (2002) 8966.
[15] S.W. Lovesey, Theory of Neutron Scattering from Condensed Matter, Clarendon, Oxford, 1984.
[16] <http://www.ncnr.nist.gov/resources/n-lengths/>.
[17] F. Mezei, The Principles of Neutron Spin Echo, vol. 112, Springer, Grenoble, 1979.
[18] B. Frick, B. Farago, in: P. Sabattier (Ed.), Scattering, vol. 2, Academic, 2002, p. 1209, Chapter 2.8.4.

[19] M. Bée, Quasielastic Neutron Scattering, Adam Hilger, Bristol, 1988.
[20] K. Chrissopoulou, S.H. Anastasiadis, E.P. Giannelis, B. Frick, in press.
[21] B. Frick, L.J. Fetters, Macromolecules 27 (1994) 974.
[22] R. Zorn, B. Frick, L.J. Fetters, J. Chem. Phys. 116 (2002) 845.
[23] B. Frick, D. Richter, W. Petry, U. Buchenau, Z. Phys. B 70 (1988) 73.
[24] M. Prager, A. Heidemann, Chem. Rev. 97 (1997) 2933.
[25] J. Colmenero, R. Mukhopadhyay, A. Alegría, B. Frick, Phys. Rev. Lett. 80 (1998) 2350.
[26] A.J. Moreno, A. Alegría, J. Colmenero, M. Prager, H. Grimm, B. Frick, J. Chem. Phys. 115 (2001) 8958.
[27] A.J. Moreno, A. Alegría, J. Colmenero, B. Frick, Phys. Rev. B 65 (2002) 134202.
[28] A.J. Moreno, J. Colmenero, A. Alegría, C. Alba-Simionesco, G. Dosseh, D. Morineau, B. Frick, Eur. Phys. J. E 12 (2003) S43.
[29] S.H. Anastasiadis, K. Karatasos, G. Vlachos, E. Manias, E.P. Giannelis, Phys. Rev. Lett. 84 (2000) 915.
[30] B. Frick, in: M. Giordano, D. Leporini, M.P. Tosi (Eds.), Non-Equilibrium Phenomena in Supercooled Fluids, Glasses and Amorphous Materials, World Scientific, 1995, p. 255.
[31] V. Arrighi, F. Ganazzoli, C.H. Zhang, S. Gagliardi, Phys. Rev. Lett. (2003) 90, art. no. 058301.
[32] V. Arrighi, S. Gagliardi, C. Zhang, F. Ganazzoli, J.S. Higgins, R. Ocone, M.T.F. Telling, Macromolecules 36 (2003) 8738.
[33] A. Schönhals, this volume.
[34] A. Schönhals, H. Goering, C. Schick, B. Frick, R. Zorn, Eur. Phys. J. E 12 (2003) 173.
[35] A. Schönhals, H. Goering, C. Schick, B. Frick, R. Zorn, Mat. Res. Soc. Symp. Proc. 790 (2004) 9.3.1.
[36] A. Schönhals, H. Goering, C. Schick, B. Frick, R. Zorn, Colloid Polym. Sci. 282 (2004) 882.
[37] C. Alba-Simionesco, G. Dosseh, E. Dumont, B. Frick, B. Geil, D. Morineau, V. Teboul, Y. Xia, Eur. Phys. J. E 12 (2003) 19.
[38] B. Frick, D. Richter, Science 267 (1995) 1939.
[39] B. Frick, K. Dalnoki-Veress, J.A. Forrest, J. Dutcher, C. Murray, A. Higgins, Eur. Phys. J. E 12 (2003) S93.
[40] A. Schönhals, R. Zorn, B. Frick, in press.
[41] G. Dosseh, C. Le Quellec, C. Alba-Simionesco, et al., in press.
[42] Y. Inamura, M. Arai, O. Yamamuro, A. Inaba, N. Kitamura, T. Otomo, T. Matsuo, S.M. Bennington, A.C. Hannon, Physica B 263 (1999) 299.
[43] Y. Inamura, M. Arai, T. Otomo, N. Kitamura, U. Buchenau, Physica B 284 (2000) 1157.
[44] B. Frick, C. Alba-Simionesco, J. Hendricks, L. Willner, Progr. Theor. Phys. Suppl. 126 (1997) 213.
[45] B. Frick, G. Dosseh, A. Cailliaux, C. Alba-Simionesco, Chem. Phys. 292 (2003) 311.
[46] R. Zorn, L. Hartmann, B. Frick, D. Richter, F. Kremer, J. Non-Cryst. Solids 307 (2002) 547.
[47] T. Asthalter, M. Bauer, U. van Burck, I. Sergueev, H. Franz, A.I. Chumakov, Eur. Phys. E 12 (2003) S9.
[48] R. Zorn, B. Frick, L. Hartmann, F. Kremer, D. Richter, Physica B (2004) 350.
[49] R. Zorn, A. Schönhals, B. Frick, in press.
[50] K. Chrissopoulou, A. Afratis, S.H. Anastasiadis, B. Frick, in press.